J. Marine Sci. Appl. (2016) 15:73-85
DOI: 10.1007/s11804-016-1344-z

Rapid Prediction of Structural Responses of Double-Bottom Structures in Shoal Grounding Scenario

Zhiqiang Hu[1*], Ge Wang[2], Qi Yao[1], and Zhaolong Yu[3]

1. State Key Laboratory of Ocean Engineering, Shanghai Jiao Tong University, Shanghai, 200240,China
2. Jiangsu University of Science and Technology, Zhenjiang, 212003, China
3.Department of Marine Technology, Norwegian University of Science and Technology, Trondheim, NO-7491, Norway

Abstract: This study presents a simplified analytical model for predicting the structural responses of double-bottom ships in a shoal grounding scenario. This solution is based on a series of analytical models developed from elastic-plastic mechanism theories for different structural components, including bottom girders, floors, bottom plating, and attached stiffeners. We verify this simplified analytical model by numerical simulation, and establish finite element models for a typical tanker hold and a rigid indenter representing seabed obstacles. Employing the LS-DYNA finite element solver, we conduct numerical simulations for shoal-grounding cases with a wide range of slope angles and indentation depths. In comparison with numerical simulations, we verify the proposed simplified analytical model with respect to the total energy dissipation and the horizontal grounding resistance. We also investigate the interaction effect of deformation patterns between bottom structure components. Our results show that the total energy dissipation and resistances predicted by the analytical model agree well with those from numerical simulations.

Keywords: shoal grounding, simplified analytical method, numerical simulation, structural response, energy dissipation, resistance

Article ID: 1671-9433(2016)01-0073-13

1 Introduction

In recent decades, sea traffic has steadily increased, which has led to an increased risk of ship collisions and groundings, and associated great economic loss, severe environmental pollution, and loss of human life. In one example on February 15, 1996, the grounding accident of the Sea Empress spilled 72,000 tons of crude oil in the Milford Haven Waterway in Pembrokeshire, Wales, resulting in the deaths of thousands of birds, shore seaweeds, and invertebrates, and great economic loss. Grounding disasters with severe consequences cause wide public concern, and there is a demand for more appropriate tools and design regulations regarding collision and grounding in order to enhance sailing safety and to protect the marine environment.

Received date:2015-09-20
Accepted date:2015-12-15
Foundation item: This work is financially supported by the National Natural Science Fundation of China (Grant No. 51239007)
***Corresponding author Email:** zhqhu@sjtu.edu.cn

The need to improve the structural crashworthiness of ships and offshore structures has been emphasized by the International Ships and Offshore Structures Congress (ISSC 2015). To enhance the crashworthiness of ships, there must be a thorough understanding of the structural deformation mechanisms and responses during ship collision, and grounding, which depend mainly on the scantlings and arrangements, the nature of loads, and the boundary conditions (Simonsen and Wierzbicki, 1997). If a ship runs aground at a forward speed, it is termed as "powered grounding" (Simonsen and Friis-Hansen, 2000). The mechanics involved in a powered grounding vary due to the variety of seabed topologies. The shape and size of the striking objects are also crucial parameters affecting structural behavior. According to Alsos and Amdahl (2007), seabed obstacles can be divided into three categories: rock, reef, and shoal, as shown in Fig. 1.

Of these three, rock-type seabed obstacles may lead to the shear and tensile failure of plates, which then result in the tearing or cutting of plates. Many investigations have been conducted regarding plate-tearing failure modes, including papers by Vaugnan (1980), Ohtsubo and Wang (1995), Zhang (2002), Wang *et al.* (2000, 2002),Liu *et al*.(2013), and Zeng *et al*.(2014). Shoal-type seabed obstacles are the most common (Amdahl *et al*. 1995; Wang *et al*. 2000, 2002), and the global hull-bending capacity of the wreck ship is reduced in shoal-grounding accidents, which may lead to the collapse of the hull girder with hazardous consequences (Alsos and Amdahl, 2008). Presently, however, there is a scant research on ship structural responses during shoal-grounding accidents, as compared with that on rock-type grounding accidents. Therefore, this study addresses the structural responses of double-bottom structures in shoal-grounding accident scenarios.

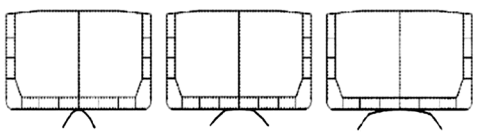

(a) rock (b) reef (c) shoal

Fig. 1 Seabed obstacles (Alsos and Amdahl, 2007)

There are four prevalent approaches for estimating

structural responses during ship collision and grounding, including empirical methods, experimental methods, simplified analytical methods, and Nonlinear Finite Element Methods (NLFEM).

Compared to the other three approaches, simplified analytical methods provide a deep understanding of the deformation mechanism. In addition, simplified analytical methods are mathematically tractable and can predict results rapidly and with reasonable accuracy, while physical and numerical experiments are relatively more time-consuming as well as expensive. As such, in the preliminary design phase, simplified analytical methods are convenient for making a quick assessment of a ship's structural performance during collision and grounding, where various designs must be quickly checked and compared with respect to a variety of potential accident scenarios. Based on the reconstruction of the deformation mechanisms identified during actual ship accidents, many innovative simplified analytical methods have been developed. Vaughan (1980), Ohtsubo and Wang (1995), Thomas and Wierzbicki (1992), Simonsen and Pedersen (1997), Hong and Amdahl (2008), and Liu *et al.* (2015) have allproposed unique simplified analytical methods for assessing the structural performances of ships during collision and grounding.

Hong and Amdahl (2013) developed simplified analytical models for three plating types during shoal grounding, including longitudinal girders, transverse floors, and outer bottom plating. Hu *et al.*(2011) conducted verification studies of the plating of a double-bottom tanker with respect to energy dissipation and grounding resistance. However, this work only tested cases with one indenter slope and shallow indentations. Furthermore, the prevailing method for dealing with stiffeners is the smeared thickness method, which cannot capture the true deformation mechanism characteristics of stiffeners. To clearly identify the deformation mechanism of attached stiffeners, Yu *et al.*(2013a,b,c) developed simplified analytical methods to determine performance during shoal-grounding accidents for three types of stiffeners attached to girders, floors, and outer bottom plating.

In addition to analytical methods, numerical simulation methods have also contributed a great deal to the analysis of ship collision and grounding. With the rapid advances being made in memory capacity and CPU performance, numerical simulations of the nonlinear elastic–plastic response of complicated hull structures are now practicable (Kitamura, 2002). Measures of energy dissipation, structural stresses, resistance, and other factors can be obtained with high accuracy, when due consideration is given to mesh size and other critical parameters in the numerical code. In addition, finite element models can be recycled several times and various aspects of the results can be analyzed repeatedly on demand. However, numerical simulation remains a time-consuming process, which cannot be conveniently applied to rapidly assess the structural performances of ship bottom structures during shoal grounding. Therefore, numerical simulations are used here to verify our proposed simplified analytical model.

In this study, we propose and verify an integrated simplified analytical method based on two existing methods by Hong *et al.* and Yu *et al.*for predicting the structural performance during shoal grounding of each of the main bottom structural components. We perform a comprehensive verification using LS-DYNA simulation software. The numerical simulation contains cases covering a wide range of indenter slope angles and indentation depths. We obtain the energy dissipation and grounding resistances to perform the assessment. We obtained good agreements and were able to verify the efficacy of the simplified analytical method. We also identified and studied the interaction effect of the deformation patterns between the structural components. The proposed analytical method can be conveniently used to make fast and reliable assessments of typical double-bottom ship structures during shoal grounding accidents in various scenarios, which is expected to be especially useful in the preliminary design phase and in emergency situations.

2 Simplified analytical models

2.1 Simplified analytical models for double-bottom structural components

The major structural components in a grounding process include three types of plating as follows: longitudinal girders, transverse floors, and outer bottom plating, as well as three corresponding kinds of stiffeners that are attached to them.

As noted above, Hong and Amdahl (2013) developed simplified analytical models for these three structural component types. Yu *et al.* (2013a,b,c) then developed simplified analytical models for the corresponding attached stiffeners. We now propose a simplified analytical method for assessing the structural performance of ship bottom structures during shoal grounding based on an integration of these models with respect to the major structural components. With this integrated model, we can obtain the total energy dissipation and grounding resistance.

2.1.1 Simplified analytical model for longitudinal girders

Girders are crushed both vertically and horizontally during the sliding process of ship grounding. Hong and Amdahl (2008) developed a simplified analytical model for girders crushed by a flat indenter during horizontal sliding. In practice, the intersection between the girders and floors can be considered to be a plated cruciform. However, for simplicity, the horizontal sliding model can be applied to whole girders, neglecting the interaction between the girders and floors. The energy dissipation of a girder in half a wave can be obtained using the theoretical model by Hong and Amdahl (2008), as follows:

$$E_{\text{girder}} = M_{0\_\text{girder}}\pi H(1+2\sqrt{1+\tan^2\theta})\cdot\frac{1-\tan^2\theta}{\tan\theta}+\frac{4N_{0\_\text{girder}}H^2}{\sqrt{3}}\sqrt{\frac{1}{4}+\tan^2\theta} \quad (1)$$

where M_0 represents the fully plastic bending-moment capacity of a plate strip and N_0 represents the corresponding plastic membrane force of a plate strip. H and θ are half of the vertical crushing distance and the crushing wave angle of the mechanism, respectively. They are empirically determined as follows:

$$2H = 1.0836D + 0.0652 \tag{2}$$

$$2\theta = 0.94\alpha - 0.0048\alpha^2 \tag{3}$$

where D is the indentation depth of the indenter and α is the slope angle of the indenter.

2.1.2 Simplified analytical model for transverse floors

The floors can be divided into their central and side parts, according to their responses. The deformation mode of the central floor part, which has the same width as the contact surface of the indenter, is similar to the vertical axial crushing of the intersections, neglecting the horizontal displacement. The central floor part is considered to be two flanges of a cruciform. The side floor part deforms with the central part simultaneously, but the deformation mode is similar to that of the local denting mode of a web girder subjected to a concentrated load. The energy dissipation can be calculated by adding together the computations for each floor part (Hong and Amdahl, 2013) as follows:

$$E_{\text{floor,central}} = 4M_{0\_\text{floor}}\left(2.58\frac{H^2}{t} + \left(\frac{\pi}{2}\right)^2 + \pi C\right) \tag{4}$$

$$E_{\text{floor,side}} = \frac{14}{3}\pi M_{0\_\text{floor}} b + 29.68\frac{N_{0\_\text{floor}}H^3}{b} \tag{5}$$

where C is the half-span of the contact surface of the indenter, and b is the half-length of the transverse deformation extension. According to the upper-bound theorem, b can be calculated as follows:

$$b = 2.85H\sqrt{\frac{H}{t_{\text{floor}}}} \tag{6}$$

where t_{floor} is the thickness of the floor.

2.1.3 Simplified analytical model for outer bottom plating

The outer bottom plating is indented by the shoal-type seabed obstacle without any tearing or cutting of the plates. Neglecting the minor effect of other components on the deformation of the outer bottom plating, the deformation pattern of the outer bottom plating within the breadth of the flat upper surface of the indenter is the same for any arbitrary section and has the same magnitude of horizontal displacement. The energy dissipation of the outer bottom plating is mainly dissipated via the following three modes: plastic bending about the longitudinal hinge lines, membrane stretching, and plastic rolling. For a crushing length l, the total energy dissipated by outer bottom plating is determined as follows (Hong and Amdahl, 2013):

$$E_{\text{plating}} = 4l\left(M_{0\_\text{plating}}\Delta\varphi + \frac{N_{0\_\text{plating}}}{\sqrt{3}}\sqrt{u_0^2 + v_0^2} + \frac{2M_{0\_\text{plating}}C}{R}\right) \tag{7}$$

where R is the radius of the rolling process, and u_0 and $v_0$are the horizontal and transverse displacements of the plate, respectively. From experience, R can be set as 1 000 mm. u_0 and v_0 can be calculated as follows:

$$u_0 = D\tan\theta \tag{8}$$

$$v_0 = \sqrt{D^2 + b^2} - b \tag{9}$$

$\Delta\psi$ indicates the bending angle of the plate in contact with the side surface of the indenter, which is expressed as follows:

$$\Delta\psi = \arctan\left(\frac{D}{b}\right) \tag{10}$$

2.1.4 Simplified analytical model for stiffeners on girders

The stiffeners used on girders can be divided into two categories based on their extent of contact as follows: fully contacting stiffeners and indirectly contacting stiffeners, which do not touch the indenter directly but deform in a way that corresponds with the deformation of the girders.

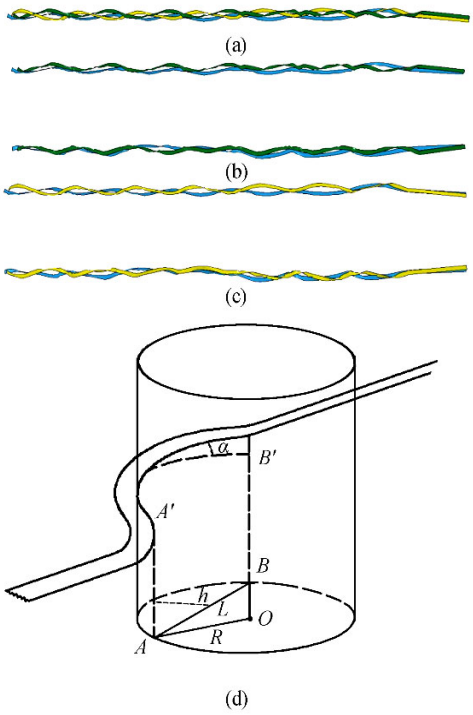

(a) Deformation mode of top girder stiffeners
(b) Deformation mode of middle girder stiffeners
(c) Deformation mode of low girder stiffeners
(d) Structural deformation of fully contacting stiffener

Fig. 2 Deformation of stiffeners on one girder (top) and a schematic of the theoretical model for fully contacting stiffeners (bottom) (Yu *et al.*, 2013a)

Fig. 2 shows the deformation patterns of stiffeners on one girder and a schematic of a simplified analytical model for fully contacting stiffeners. The cylindrical contour guarantees that the stiffeners will have the same transverse extension. To calculate the reduced transverse extension for indirectly contacting stiffeners, we simplify the deduction of

the transverse extension by introducing a strip beam model with one end rigidly fixed and the other bearing a bending moment. Then, we can obtain the energy dissipation in a similar way to that of the fully contacting stiffeners.

It is crucial that the horizontal and vertical deformation periodicities be determined. We observe from numerical simulations that the horizontal cycle length of the deformation mode for stiffeners on girders approximately approaches the interval between adjacent transverse floors under different slope angles and indentation conditions. Therefore, we can assume that the horizontal cycle length is a constant value, $Lc = 2L$. When the indentation grows to a certain value set as $2H_0$, a new vertical cycle begins, and the maximum transverse extension will slowly increase. A closed form solution for H_0 is temporarily unavailable, and expressions are given based on numerical simulations as follows:

$$2H_0 = \begin{cases} 0.45H_b, \alpha < 45\deg \\ 0.60H_b, \alpha \geq 45\deg \end{cases} \tag{11}$$

According to Yu *et al*. (2013a), in fully contacting stiffeners, the energy dissipation in half a horizontal cycle is obtained as follows:

$$E_{gs,L} = \frac{M_{0,1\_gs} t_{gs} L\varphi^2}{\sin\varphi} + N_{0\_gs} \cdot \left(\frac{2R_{gs}\varphi}{\cos\theta} - L \right) + 2M_{0,2\_gs} h_{gs} L\alpha \tag{12}$$

For indirectly contacting stiffeners, the energy dissipation in half a horizontal cycle is expressed as follows:

$$E_{gs,L} = \frac{M_{0,1\_gs} t_{gs} L\varphi^2}{\sin\varphi} + N_{0,1\_gs} \cdot (2R_{gs}\varphi - L) \tag{13}$$

where $h_{gs}$and t_{gs} are the height and thickness of the girder stiffener, respectively. $M_{0,1\_gs}$ and$M_{0,2_gs}$ are the fully plastic bending-moment capacities of a plate strip in different directions, expressed as follows:

$$M_{0,1\_gs} = \frac{\sigma_{0,gs} h_{gs}^2}{4}, M_{0,2\_gs} = \frac{\sigma_{0,gs} t_{gs}^2}{4} \tag{14}$$

2.1.5 Simplified analytical model for stiffeners on floors

In contrast to the deformation under axial crushing loads, stiffeners on floors are found to have a horizontal displacement in shoal grounding. Additionally, the displacement tends to increase as the indentations increase. Based on the response of the floor stiffeners in numerical simulations, we can establish theoretical models using the strip beam theory, as shown in Fig. 3.

Based on the geometrical relationship in the theoretical models and the plastic deformation mechanisms, we can obtain the energy dissipation of the stiffeners (Yu *et al*., 2013b).

When $D < Ls/2$, the energy dissipation of a stiffener can be calculated as follows:

$$E_{fs} = \frac{M_{0\_fs} t_{fs} x_1 \psi^2}{\sin\psi} + \frac{M_{0\_fs} t_{fs} x_1 (2\beta - \psi)^2}{\sin(2\beta - \psi)} + 2N_{0\_fs}\beta h_{fs} + 4M_{0\_fs} t_{fs}\beta \tag{15}$$

When $Ls/2 \leqslant D \leqslant 3Ls/4$, the energy dissipation of a stiffener can be calculated as follows:

$$E_{fs} = \frac{M_{0\_fs} t_{fs} x_1 \psi^2}{\sin\psi} + \frac{M_{0\_fs} t_{fs} x_2 (2\beta - \psi + \pi/2)^2}{\cos(2\beta - \psi)} + N_{0\_fs}\left(2\beta + \frac{\pi}{2}\right) h_{fs} + M_{0\_fs} t_{fs}(4\beta + \pi) \tag{16}$$

Details for the parameters x_1, x_2, β, and ψ can be found in the study by Yu*et al*. (2013b).

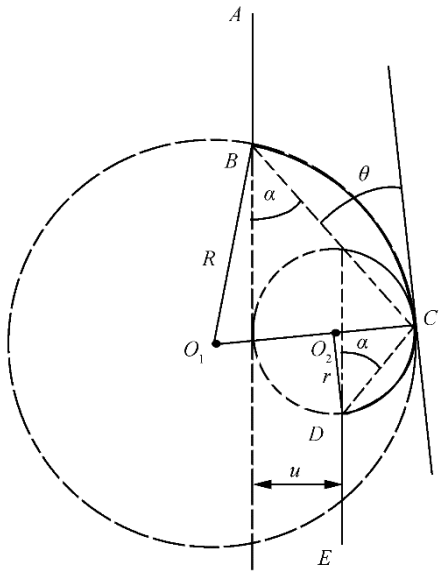

(a) Deformation mode of floor stiffeners when $D < Ls/2$

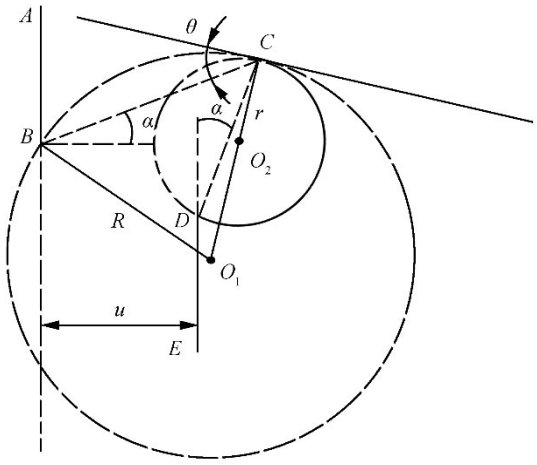

(b) Deformation mode of floor stiffeners when $Ls/2 <= D < 3Ls/4$

Fig. 3 Schematics of theoretical models for floor stiffeners during shoal (Yu *et al*., 2013b)

When D is larger than $3Ls/4$, the theoretical model is invalid. Therefore, we can assume that the energy dissipation can be determined by summing the basic and the additional energies. The basic energy denotes the energy dissipation at the basic indentation $3Ls/4$. The additional energy is that dissipated through plastic bending around the

hinge line rotating 180 degrees as follows:

$$E_{\text{additional}} = M_{0\_fs} t_{fs} (D - D_{\text{basic}})\pi \tag{17}$$

$$E_{fs} = E_{\text{additional}} + E_{\text{basic}} \tag{18}$$

Additionally, due to the interaction effect between the bending moment and membrane stretching in actual yield conditions, and the three-dimensional deformation in actual deformation mode, which are all ignored in the simplified analytical model, a greater energy dissipation is inevitable. Consequently, we apply the energy reduction coefficient λ, as determined from experience as follows:

$$\lambda = \begin{cases} 0.714, & D < L_s / 2 \\ 0.833, & D > L_s / 2 \end{cases} \tag{19}$$

2.1.6 Simplified analytical model for stiffeners on outer bottom plating

Fig. 4 presents the deformation and the theoretical model for stiffeners on outer bottom plating. We clearly observe from the numerical simulations that the deformation pattern is periodic. The cycle length is assumed to be as follows: $L_c = D / \sin\alpha$

We also considered plastic rolling deformations at two major rollers. The energy is mainly dissipated in the following three patterns:

1) Plastic rolling in contact with the front surface of the indenter (Roller 1 and Roller 2);

2) Membrane stretching (Roller 2);

3) Local tripping of the stiffeners.

In contrast to Roller 1, which is mainly influenced by the bending moment, Roller 2 is subjected to the combined actions of bending moment and axial force due to the friction force. Compared with the other two patterns, the local tripping effect contributes very little to energy dissipation. By summing the values of the energy dissipated through the three patterns above, we can obtain the energy dissipation of the outer bottom plating stiffener (Yu *et al*., 2013c).

When the ship slides over a length L_c, the energy dissipation of a stiffener can be calculated as follows:

$$E_{ps} = M_{0,1\_ps} t_{ps} \frac{L_c}{R_{ps}} + \frac{\pi^2 M_{0,2\_ps} h_{ps}^2 \alpha}{8(\pi - 2)} + M_{0,1\_ps} t_{ps} \frac{L_c}{R_{ps}} + M_{0,1\_ps} t_{ps} \left(\frac{N_{ps}}{N_{0\_ps}} \right)^2 \frac{L_c}{R_{ps}} \tag{20}$$

where R_{ps} is the radius of plastic rolling, and N is the axial membrane stretching force of one stiffener. These parameters are expressed as follows:

$$N = \frac{F_{\text{friction}}}{n} = \frac{\mu P}{n} \tag{21}$$

$$R_{ps} = 1 / \alpha \tag{22}$$

where n is the number of stiffeners involved, and P is the grounding resistance normal to the contact surface. Because the ratio of N to N_0 should never be larger than 1 in any situation, it is set as 1 if the calculated value N exceeds N_0. We emphasize that the unknown parameter P is required for calculating the energy dissipation of the outer bottom plating stiffeners, while the energy dissipated by the stiffeners also has an effect on P. Thus, there is an obvious interaction effect between grounding resistance and energy dissipation.

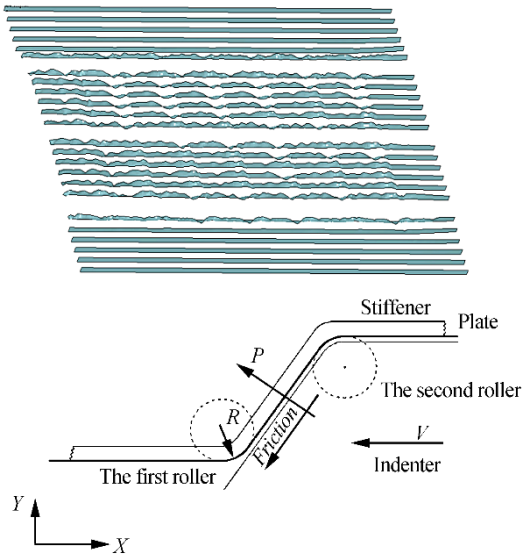

Fig. 4 Deformation (top) and schematic of the theoretical model for stiffeners on outer bottom plating (bottom) during shoal grounding (Yu *et al*., 2013c)

2.2 Total energy dissipation and grounding resistance

Combining the equations above, we obtain the total energy dissipated through the bottom structures due to plastic deformation as follows:

$$E_{\text{plasticity}} = E_{\text{girder}} + E_{\text{floor,central}} + E_{\text{floor,side}} + E_{\text{plating}} + E_{gs} + E_{fs} + E_{ps} \tag{23}$$

The relations between total energy dissipation and grounding resistance are derived as follows:

$$E_{\text{total}} = F_{H,\text{plasticity}} \cdot l + F_{V,\text{plasticity}} \cdot D \tag{24}$$

$$F_{V,\text{plasticity}} = F_{H,\text{plasticity}} / \tan\alpha \tag{25}$$

where $F_{H,\text{plasticity}}$ and $F_{V,\text{plasticity}}$ are the average horizontal resistance and the vertical resistance in relation to the plastic deformation of the structures, respectively.

Friction plays an important role in the grounding process. The horizontal grounding resistance in terms of $F_{H,\text{plasticity}}$ is expressed as follows:

$$F_H = \left(1 + \frac{u}{\tan\alpha}\right) \cdot F_{H,\text{plasticity}} \tag{26}$$

Based on the balance of forces, the vertical grounding resistance F_V, and the combined grounding force P are derived as follows:

$$F_V = \left(\frac{1}{\tan\alpha} - u\right) F_{H,\text{plasticity}} \tag{27}$$

$$P = \sqrt{F_{H,\text{plasticity}}^2 + F_{V,\text{plasticity}}^2} \tag{28}$$

where μ is the friction coefficient, which is often taken as 0.3. We determine the interaction effect between the grounding resistance and the total energy dissipation byEq.(20). Therefore, to obtain precise results, we employ an iterative cycle calculation process, as shown in Fig. 5.

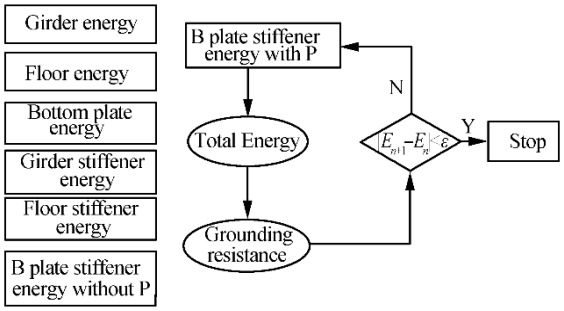

Fig.5 Calculation flow diagram

However, the horizontal grounding resistance predicted by the simplified methods is obviously smaller than the actual values because the elastic component during shoal grounding was disregarded. Experientially, the elastic component is assumed to be proportional to the plastic component, and the proportionality coefficient is assumed only to relate to the indentation, ignoring the minor effect of slope angle. Therefore, the horizontal grounding resistance is modified experientially by multiplying it with a coefficient κ, which is expressed as follows:

$$\kappa = 0.27D + 1.1 \tag{29}$$

3 Comparison with numerical simulation

3.1 Numerical models

We chose a double-bottom tanker with a 140 000 ton displacement for the case study, and its scantling details are listed in Table 1. First, we established a finite element model of the tanker hold. Then, we used the explicit solver LS-DYNA version 971 to calculate structural performance during ship grounding.

Table 1 Scantling of the double bottom of the tanker / m

Item	Value
Total length	265.0
Scantling breadth	42.5
Scantling height	22.0
Scantling draught	16.5
Length of one hold	32.0

We modeled the tank hold and indenter using quadrilateral Belytschko-Lin-Tsay shell elements. We defined the deformation regions containing the longitudinal girders, floors, outer bottom plating, and the attached stiffeners as having elastic-plastic properties. With respect to calculation accuracy and computational costs, we defined the mesh size of the deformation area as 120 mm× 120 mm. Although the deformation of the inner bottom plating, brackets, and the middle girder above the inner bottom plating is small, we also meshed them with fine meshes and defined them as having elastic-plastic properties, as they influence the deformation of the large deformation region.

The shoal-type seabed is represented by an indenter with a trapezoidal cross section and flat sides. The length of the side of the indenter top surface is just larger than the span of the middle three girders so that the three girders can deform in each case. The indenter is defined as rigid and slides longitudinally along the bottom structures at a constant prescribed speed of 5 m/s.

We defined material failure in the model using the strain failure criterion based on practical grounding accidents. During the simulation, we defined the contact between the indenter and the outer bottom plating as master-slave contact, while we defined the contact between each part of the bottom structures as self-contact. We considered the static friction coefficient for the contact as well and defined it as 0.3.

The indenter is only free in the longitudinal direction, while the rigid area of the hold is constrained within six degrees of freedom. Fig. shows the grounding scenario of the finite model.

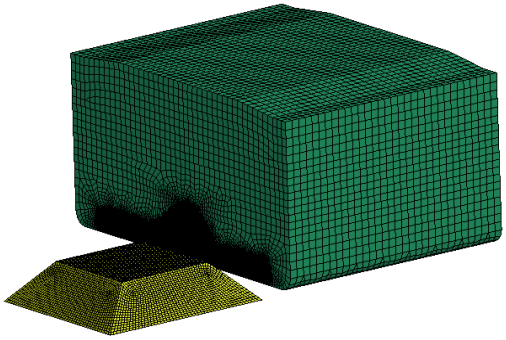

Fig.6 Grounding scenario of the finite model

3.2 Simulation cases

The slope angle and indentation depth of the indenter are the two main parameters that greatly influence the deformation of bottom structures. In the shoal-type seabed, the slope angle is not very large. However, to comprehensively investigate the deformation of bottom structures, we employed indenter slope angles of 20, 26.5, 45, and 60 degrees in the simulation cases. For a given angle, the indenter depth varies from 10% to 90% of the height of the double bottom H_b. D is indentation. The simulation case M25 represents a slope angle of 20 degrees and an indentation of $0.5H_b$. There were a total of 24 cases, as

detailed in Table 2.

Table 2 Case parameter details

Model	α/(°)	*D* /m	D/H_b / %
M21	20	0.268	10
M23	20	0.804	30
M25	20	1.340	50
M27	20	1.876	70
M29	26.5	2.412	90
M31	26.5	0.268	10
M33	26.5	0.804	30
M35	26.5	1.340	50
M37	26.5	1.876	70
M39	26.5	2.412	90
M41	26.5	0.268	10
M42	26.5	0.536	20
M43	45	0.804	30
M44	45	1.072	40
M45	45	1.340	50
M46	45	1.608	60
M47	45	1.876	70
M48	45	2.144	80
M49	45	2.412	90
M61	60	0.268	10
M63	60	0.804	30
M65	60	1.340	50
M67	60	1.876	70
M69	60	2.412	90

3.3 Verification of the simplified analytical model for double-bottom structures

3.3.1 Deformation mode

The proposed simplified analytical model is based on the plastic mechanism and the deformation pattern identified in the numerical simulations of the major bottom components during shoal grounding. The deformations of structural components are in fact complicated—involving bending, stretching, and crushing. However, the simplified analytical model captures the major deformation characteristics while ignoring the subordinate deformations and the interaction effect between components.

Due to the periodic arrangement of the transverse structural components, the deformation patterns of the longitudinal components are also cyclic. The deformation patterns and VonMises stress fringes of the primary double-bottom structures as shown in Fig. 7, occur during the course of sliding. As we see in Fig. 7, the interaction effects of the structural deformation pattern between the longitudinal girders, the transverse floors, and the bottom plating are obvious. For example, when the rigid indenter moves in a longitudinal direction, the girder deforms like a regular wave with a constant wavelength, which is nearly the interval between the adjacent transverse floors, and the horizontal displacement of the floors at the girder-floor intersection is obviously smaller than that of other floor areas. In addition, during the deformation process, there are sunken deformation areas in the intersection between the girders and the outer bottom plating, and the floors and the bottom plating. Simultaneously, the stiffeners attached to the girders, floors, and outer bottom plating deform with the attached plating.

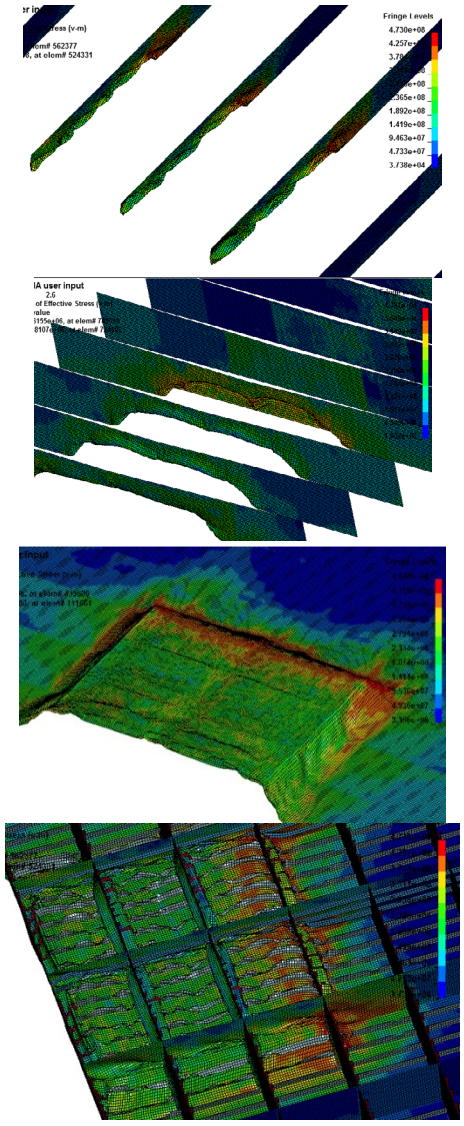

Fig.7 Deformation patterns and VonMises stress fringes of main components

To better understand the interaction of these deformations, Fig.8 shows the displacement of the nodes around the intersection.

Hong and Amdahl (2008) verified the interaction between the longitudinal and transverse members but only for the horizontal displacement effect on the girders. As such, here we make a detailed investigation of the interaction between

the girders and the floors, the outer bottom plating and the transverse floors, and the outer bottom plating and the longitudinal girders. We chose case M45 as an example to illustrate the interaction effect.

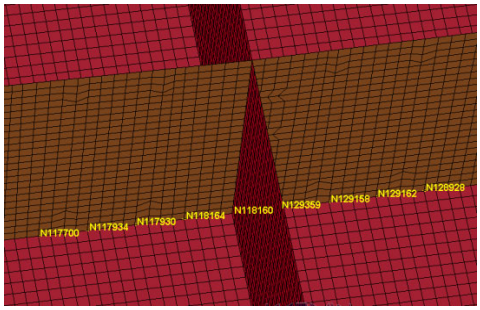

(a) Definition of the nodes on the floor at the bottom edge

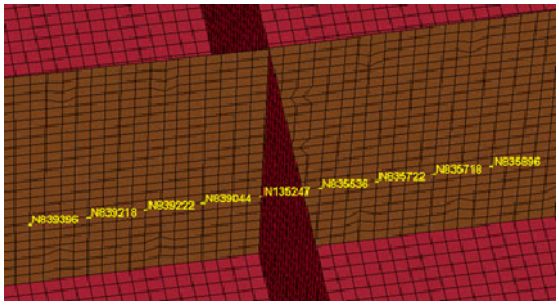

(b) Definiton of nodes on the floor far away from the bottom edge

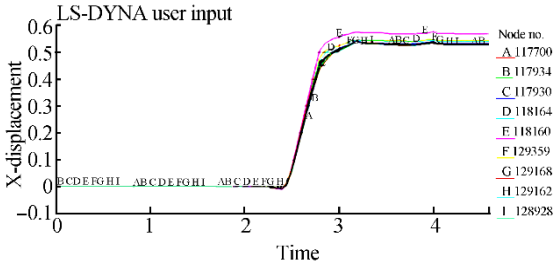

(c) Horizontal displacement value of the nodes on the floor at the bottom edge

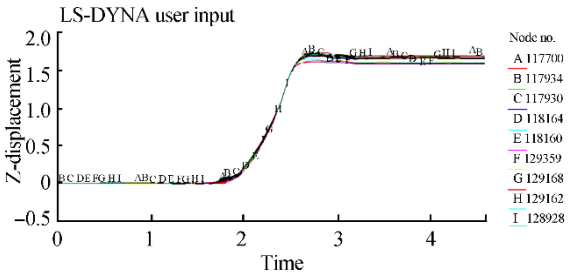

(d) Vertical displacement value of the nodes on the floor at the bottom edge

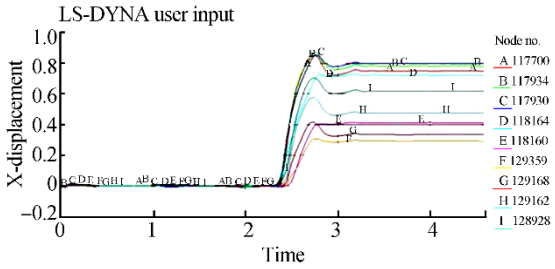

(e) Horizontal displacement value of the nodes on the floor far away from the bottom edge

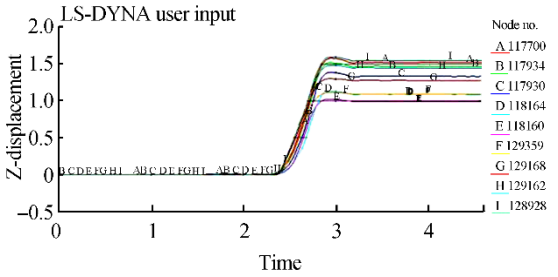

(f) Vertical displacement value of the nodes on the floor far away from the bottom edge

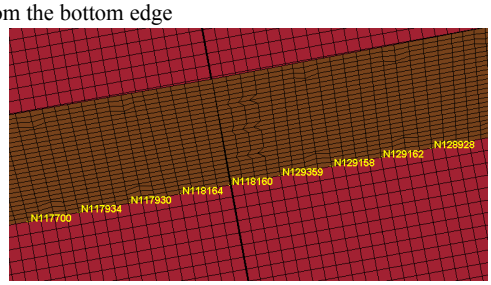

(g) Defintion of nodes on the bottom near the intersection of floors and the outer bottom plating

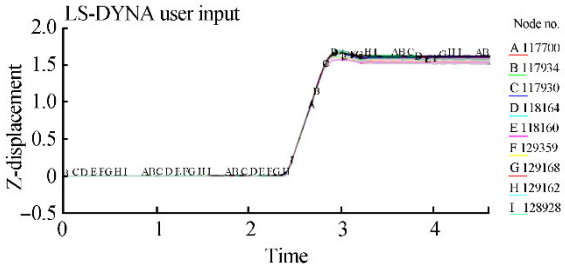

(h) Vertical displacement values of nodes on the bottom near the intersection of the floors and the outer bottom plating

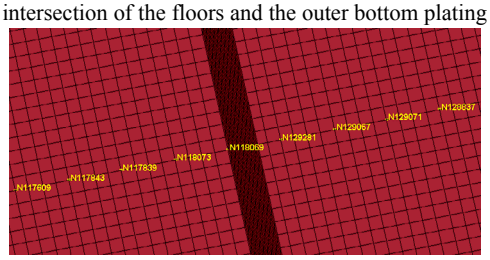

(i) Defintion of nodes on the bottom far away from the intersection of floors and the outer bottom plating

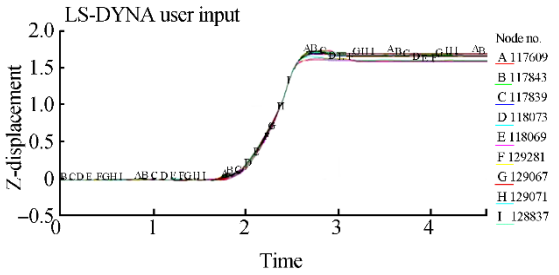

(j) Vertical displacement of the nodes on the bottom far away from the intersection of floors and the outer bottom plating

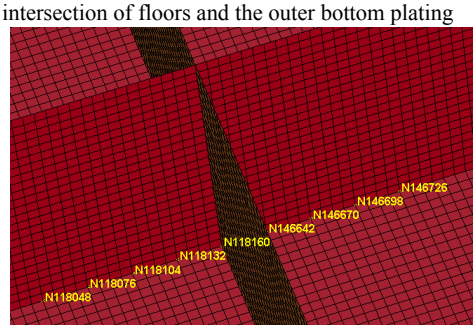

(k) Defintion of the nodes on the bottom near the intersection of the girders and the outer bottom plating

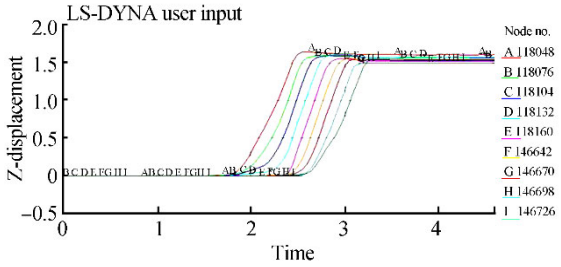

(l) Vertical displacement values of the nodes on the bottom near the intersection of the girders and the outer bottom plating

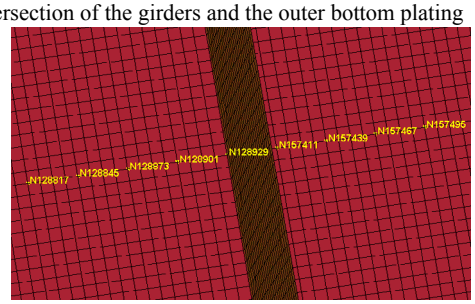

(m) Defintion of the nodes on the bottom far away from the intersection of the girders and the outer bottom plating

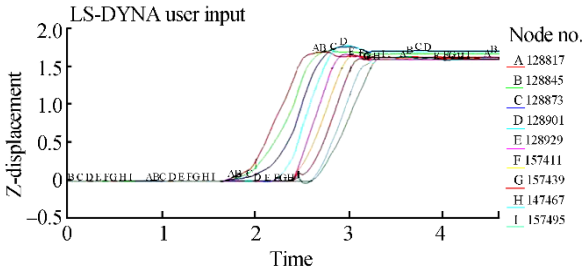

(n) Vertical displacement values of the nodes on the bottom far away from intersection of girders and outer bottom plating

Fig. 8 Displacement of different nodes for case M45

We can see from Fig.8 that the nodes at the bottom edge of the floors displace horizontally with the same magnitude. The same is true for the vertical displacement of the nodes at the bottom edge of the floors. However, the inner nodes behave differently. The nodes on the floors near the floor-girder intersection have obviously smaller horizontal and vertical displacements than the nodes at the same height but farther away from the intersection. Specifically for the M45 case, the ratio of the maximal to the minimal displacement in the horizontal and vertical directions is about 2.5 and 1.5, respectively, for floor nodes at the same height. Therefore, we can conclude that the girders play a significant role in the deformation of the floors.We can also see from Fig. 8 that nodes on the intersections between the floors and the outer bottom plating, and between the girders and the outer bottom plating, have a slightly smaller vertical displacement than that of nodes on the outer bottom plating far away from these intersections. This phenomenon is also reflected in the sunken area around the intersections between the floors and the outer bottom plating, and at the intersections between the girders and the outer bottom plating. In addition, the nodes on the outer bottom plating within the breadth of the indenter displace horizontally with almost the same magnitude. Therefore, we conclude that the floors and girders have a negligible effect on the deformation of the outer bottom plating. Conversely, the outer bottom plating greatly influences the deformation of the floors and girders, acting as the boundary condition.

3.3.2 Energy dissipation

The energy dissipation of each component, i.e., the longitudinal girders, floors, outer bottom plating, and attached stiffeners, can be obtained by the proposed analytical model. Table 3 shows a comparison of the total energy dissipation predicted by the simplified analytical method, and that by numerical simulation.

The relative error in Table 3 is defined as:

$$\text{error} = (R_{\text{simplified,method}} - R_{\text{numerical,method}}) / R_{\text{numerical,method}} \cdot 100\% \tag{30}$$

From Table 3, we see that the energy dissipation predicted by the simplified analytical method agrees well with that by numerical simulation, despite some discrepancies in some cases.

To better understand the deformation characteristics of the grounding process, we chose case M44 as an example. Fig.9 shows the curve of energy dissipation versus crushing length for case M44, and we see that fairly good agreement is obtained. The periodic humps due to the periodic arrangement of the transverse members and the nearly linear relationship between energy dissipation and crushing length are well captured.

For a deeper understanding of energy dissipation and to analyze the error source, we studied the energy dissipation of each main component and, in Fig.10, compared the cases with slope angles of 45 degrees. We can clearly see that the energy is mainly dissipated by the longitudinal girders, outer

bottom plating, floors, and stiffeners on the outer bottom plating, and that the energy dissipation by the stiffeners attached on the floors and girders is relatively small. However, some discrepancies remain between the energy dissipation predicted by these two methods for the girders, floors, outer bottom plating, and stiffeners on the outer bottom plating, while good agreement is obtained for the energy dissipation of the stiffeners on the floors and girders. Nevertheless, it is interesting to find that the two methods agree well with respect to total energy dissipation.

Table 3 Total energy dissipation

Model	Numerical method	Simplified method	Error / %
M21	2.2E+08	2.1E+08	−8.3
M23	3.9E+08	3.4E+08	−11.8
M25	5.1E+08	4.9E+08	−2.9
M27	6.6E+08	6.7E+08	0.6
M29	7.5E+08	8.4E+08	11.1
M31	2.6E+08	2.4E+08	−7.4
M33	4.6E+08	4.1E+08	−12.2
M35	6.2E+08	5.9E+08	−4.4
M37	7.8E+08	8.0E+08	2.8
M39	8.6E+08	1.0E+09	17.2
M41	3.8E+08	3.6E+08	−4.7
M42	5.5E+08	4.9E+08	−10.0
M43	6.8E+08	6.4E+08	−6.2
M44	8.1E+08	7.9E+08	−2.3
M45	9.0E+08	9.5E+08	6.0
M46	1.0E+09	1.1E+09	7.0
M47	1.2E+09	1.3E+09	10.6
M48	1.3E+09	1.5E+09	11.6
M49	1.4E+09	1.6E+09	17.0
M61	5.2E+08	5.0E+08	−5.0
M63	9.2E+08	9.4E+08	2.2
M65	1.2E+09	1.4E+09	15.3
M67	1.6E+09	1.9E+09	21.8
M69	1.9E+09	2.4E+09	25.5

One possible reason for the discrepancies with respect to the energy dissipated by the girders and floors may be the interaction effect between them. It has been observed in numerical simulations that as indentation increases, the number of waves in the girders' deformation pattern varies from one to two in the vertical direction, while there is only one wave in the simplified analytical model. The wavelength L of the girders is almost constant and equal to the spacing of the floors in the numerical simulations. However, in the simplified analytical method, the wavelength L changes when the indentation and slope angle of the indenter vary. Also, the width h' of the girder predicted by the numerical simulations and the simplified analytical models do not agree well with each other. Table 4 compares the wave length L and width h' of the deformation model for the girders of the two methods for cases with a slope angle of 45 degrees. The simplified analytical model for girders alone, without the effect of floors, was verified in Hong's paper. However, as we see in Table 4, the floors have an obvious boundary condition effect on the shape and size of the girder deformation patterns. Conversely, the girders also act as the boundary condition affecting the deformation of the floors. But this interaction effect only happens in the numerical simulations, and not in the simplified analytical method, and may result in a larger energy dissipation of the girders in the simplified analytical method, especially for the large indention cases. We can also see from Fig. 11 and Fig. 12 that the energy dissipation predicted by the simplified analytical method tends to increase faster than that by numerical simulation when either the indentation or the slope angle increases. This is because the error of the girder energy dissipation is a predominant component of the error of the total energy dissipation, especially in cases with a large indentation and a large slope angle.

The cause of the discrepancy in the outer bottom plating energy dissipation may be that the calculation value of the rolling radius R in Eq.(7) is larger than the real value, which results in smaller calculation results. The neglect of the effect exerted by other components on the outer bottom plating may also lead to the greater energy dissipation.

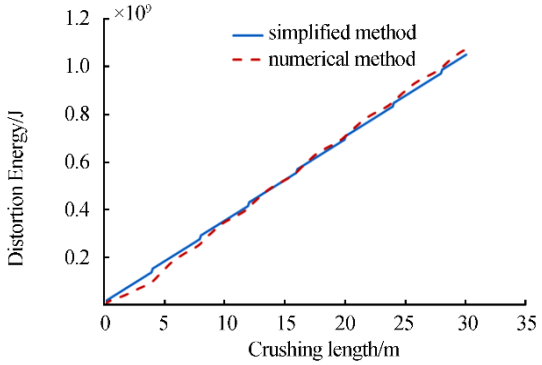

Fig. 9 Energy dissipation versus crushing length for case M44

To better illustrate the roles played by slope angle and indentation in the deformation process, we investigated cases with indentations of $0.1H_b$, $0.3H_b$, $0.5H_b$, $0.7H_b$, and $0.9H_b$, and cases with slope angles of 26.5, 45, and 60 degrees. The results are shown in Fig. 11 and Fig. 12, respectively, which capture well the basic characteristic that energy dissipation increases with the increases of slope angle and indentation. Also, the two methods agree well with respect to the energy dissipation for cases with relatively small indentations and those with small slope angles. The energy dissipation is somewhat overestimated for cases with a relatively large indentation and cases with relatively large slope angles. Nevertheless, despite these discrepancies for cases with a large indentation or slope angle, the simplified analytical method can predict the total energy dissipation with reasonable accuracy.

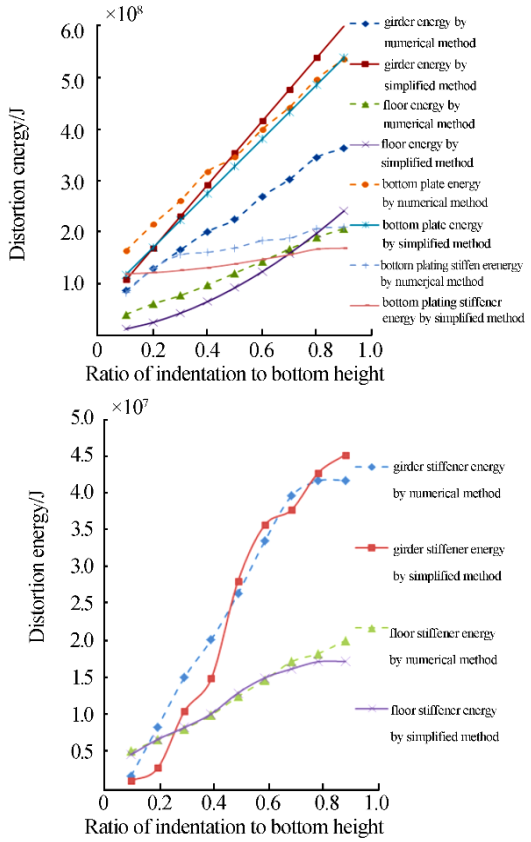

Fig. 10 Comparison of energy dissipation of six main structural components for case M44

Table 4 Comparison of wavelength and width / m

Model	Numerical simulation		Simplified analytical method	
	Wave length	Wave width	Wave length	Wave width
M41	4	0.259	0.393	0.178
M42	4	0.290	0.714	0.323
M43	4	0.322	1.035	0.468
M44	4	0.323	1.356	0.613
M45	4	0.388	1.677	0.759
M46	4	0.345	1.998	0.904
M47	4	0.482	2.319	1.049
M48	4	0.411	2.641	1.194
M49	4	0.380	2.962	1.339

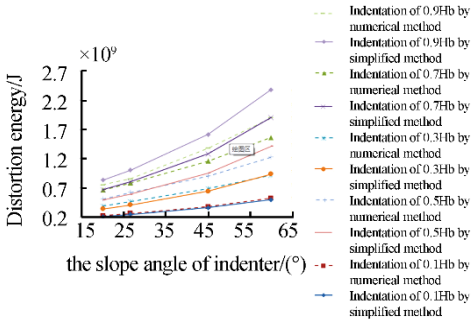

Fig. 11 Energy dissipation versus the slope angle of the indenter

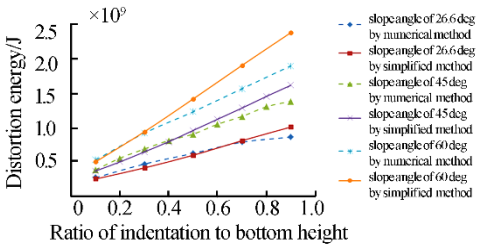

Fig. 12 Energy dissipation versus the ratio of indentation height for slope angles of 26.5, 45, and 60 degrees

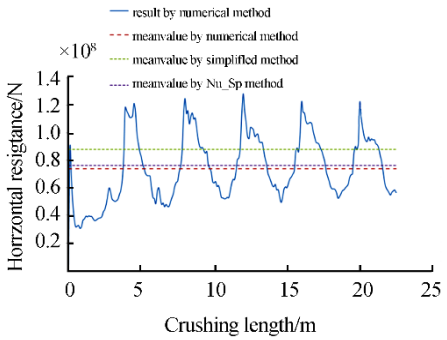

Fig. 13 Comparison of horizontal grounding resistance for case M65

3.3.3 Grounding resistance

To illustrate the characteristics of horizontal grounding resistance during grounding, Fig. 13 plots the horizontal grounding resistance versus time for case M65. We can see that in the numerical simulations, the grounding resistance oscillates periodically as the crushing length increases. In addition, the peak and trough values are nearly constant. Obviously, peak values occur when the indenter collides with the transverse floors, while trough values occur when the indenter passes the middle of adjacent floors.

According to Eq.(23), the grounding resistance is strongly related to the energy dissipation. Nevertheless, there are some discrepancies between the energy dissipation predicted by the simplified method and that by the numerical simulations. An error in the total energy dissipation may influence and be propagated to the grounding resistance, leading to further error. Therefore, to better understand the inherent and propagated errors with respect to grounding resistance, we investigated the grounding resistance, and Table 5 shows a comparison between the numerical simulation method, the simplified analytical method, and the Nu_Sp method. In the Nu_Sp method, the grounding resistance is calculated by putting the numerical energy into the simplified analytical grounding resistance formulae. We can also see from Fig. 13 that the mean horizontal resistance predicted by the Nu_Sp method agrees well with that by the numerical simulation method. Due to the propagated error of the total energy dissipation of the bottom structures, there are some discrepancies between the horizontal resistances predicted by the numerical simulated and simplified analytical methods.

The errors in Table 5 are defined in Eq.(30). Error 1 indicates a difference between the simplified analytical and

numerical simulation methods. Error 2 indicates an error between the Nu_Sp and the numerical simulation methods.

From Table 5, we see that Error 1 varies between −11.4% and 35.2%, and Error 2 varies between −9.2% and 7.7%. This implies that the simplified analytical method can predict the horizontal grounding resistance with reasonable accuracy. In addition, the horizontal grounding resistance predicted by the Nu_Sp method agrees very well with those by the numerical simulation method. This also verifies the calculation of the horizontal grounding resistance by the simplified analytical method. To better illustrate the relationship between the horizontal grounding resistance, and the slope angles of the indenter and the indentation, Fig.14 shows a comparison of the horizontal resistance predicted by the numerical simulation, the simplified analytical, and the Nu_Sp methods for cases with given indentations, and Fig.15 shows a comparison of cases with slope angles of 45 degrees. As we can see in the figures, the horizontal grounding resistance is sensitive to the indentation and the slope angle of the indenter, and increases as the indentation or slope angle increases. In addition, the larger the indentation or slope angle, the faster the horizontal grounding resistance increases. Both the Nu_Sp and simplified analytical methods capture these characteristics well.

Table 5 Horizontal grounding resistance / N

Model	Numerical method	Simplified method	Nu_Sp method	Error 1 / %	Error 2 / %
M21	2.0E+07	1.8E+07	2.0E+07	−10.4	−2.2
M23	3.4E+07	2.9E+07	3.4E+07	−15.8	−1.3
M25	4.5E+07	4.1E+07	4.4E+07	−10.3	−3.6
M27	5.9E+07	5.7E+07	5.6E+07	−4.7	−5.3
M29	7.0E+07	7.0E+07	6.3E+07	0.8	−9.2
M31	2.0E+07	1.9E+07	2.1E+07	−5.7	1.8
M33	3.6E+07	3.2E+07	3.6E+07	−11.4	1.0
M35	4.8E+07	4.6E+07	4.9E+07	−4.0	0.4
M37	6.2E+07	6.3E+07	6.1E+07	2.2	−0.7
M39	7.1E+07	7.9E+07	6.7E+07	10.9	−5.4
M41	2.5E+07	2.3E+07	2.4E+07	−6.8	−1.1
M42	3.5E+07	3.2E+07	3.6E+07	−8.5	1.6
M43	4.4E+07	4.1E+07	4.5E+07	−5.8	2.3
M44	5.2E+07	5.1E+07	5.4E+07	−1.2	3.4
M45	5.9E+07	6.4E+07	6.1E+07	9.8	3.6
M46	6.8E+07	7.6E+07	7.1E+07	11.7	4.4
M47	7.6E+07	8.8E+07	8.0E+07	15.5	4.4
M48	8.7E+07	1.0E+08	9.0E+07	15.9	3.8
M49	9.4E+07	1.1E+08	9.7E+07	20.1	2.7
M61	3.2E+07	2.9E+07	3.0E+07	−9.8	−5.0
M63	5.5E+07	5.6E+07	5.5E+07	2.4	0.2
M65	7.4E+07	8.8E+07	7.6E+07	19.2	3.3
M67	9.5E+07	1.2E+08	1.0E+08	28.1	5.2
M69	1.2E+08	1.6E+08	1.3E+08	35.2	7.7

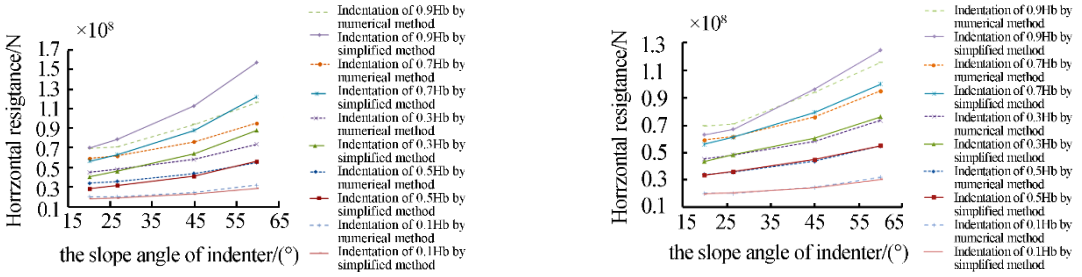

(a) (b)

Fig. 14 Comparison of average horizontal resistance for cases with given indentations

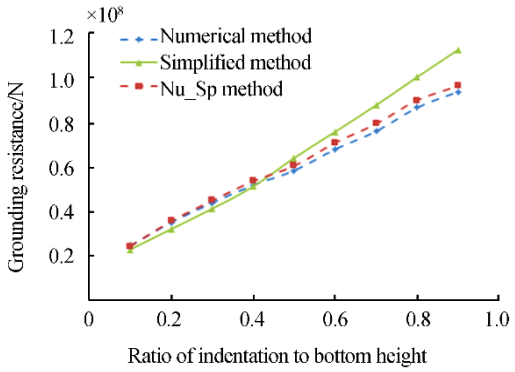

Fig. 15 Comparison of average horizontal resistance for cases with slope angles of 45 degrees

4 Conclusions

In this paper, we have introduced an integrated simplified analytical method, and a series of proposed analytical equations, for predicting the structural performance of double-bottom ship structures during shoal grounding scenarios. Through numerical simulation, we comprehensively verified the proposed simplified analytical method, and draw the following conclusions:

1) By assembling a simplified analytical model for each main double-bottom component, we established a simplified analytical model for double-bottom structures. The major deformation characteristics of the structural components are captured well in the proposed simplified analytical models.

2) The proposed simplified analytical model can predict the total energy dissipation with reasonable accuracy for a wide range of shoal shapes. In addition, the predicted horizontal grounding resistance coincides with numerical simulation results.

References

Alsos HS, Amdahl J, 2007. On the resistance of tanker bottom structures during stranding. *Marine Structures*, **20**(4), 218-237. DOI:10.1016/j.marstruc.2007.06.001

Alsos HS, Amdahl J, 2008. *Shipgrounding, analysis of ductile fracture, bottom damage and hull girder response*. Ph.D. thesis, Norwegian University of Science and Technology, Trondheim,Norway

Amdahl J, Kavlie D, Johansen A, 1995. Tanker grounding resistance. *Proc. of the Sixth Int Symposium on Practical Design of Ships and Mobil Units (PRADS1995)*,Seoul,**2**, 17-22.

Gupta NK, 2007. Deformation and tearing of circular plates with varing support conditions under uniform impulsive loads. *International Journal of Impact Engineering*,**34**(1), 42-59.

Hong L, Amdahl J, 2008. Plastic mechanism analysis of the resistance of ship longitudinal girders during grounding and collision. *J. Ships Offshore Struct.*, **3**(3), 159-171.

Hong L, Amdahl J, 2013. Rapid assessment of ship grounding over large contact surfaces. *Ships and Offshore Structures*, **7**(1), 5-19.

HuZQ, AmdahlJ, Hong L, 2011. Verification of a simplified analytical method for predictions of ship groundings over large contact surfaces by numerical simulations. *Marine Structures*, **24**(4), 436-458. DOI:10.1016/j.marstruc.2011.06.001

Kitamura O, 2002. FEM approach to the simulation of collision and grounding damage. *Marine Structures*, **15**(4), 403-428.

Liu B, Villavicencio R, Guedes Soares C, 2013. Shear and tensile failure of thin aluminum plates struck by cylindrical and spherical indenters. *Ships and Offshore Structures*, (ahead-of-print), 1-14.

Liu B, Villavicencio R, Soares CG, 2015. Simplified method for quasi-static collision assessment of a damaged tanker side panel. *Marine Structures*, **40**, 267-288. DOI:10.1016/j.marstruc.2014.11.006

Ohtsubo H, Wang G, 1995a. An upper-bound solution to the problem of plate tearing. *Journal of Marine Science and Technology*, **1**, 46-51.

Ohtsubo H, WangG, 1995b. An upper-bound solution to the problem of plate tearing. *Journal of Marine Science and Technology*, **1**(1), 46-51.

ISSC 2015, report of Committee V.1. *Accidental Limit State, International Ship and Offshore Structures Congress*, Cascais, Portugal.

Simonsen BC, Pedersen PT, 1997. *Mechanics of ship grounding*. Ph.D. thesis, Technical University of Denmark, Copenhagen, Danmark.

Simonsen BC, Wierzbicki T, 1997. Plasticity, fracture and friction in steady state plate cutting. *International Journal of Impact Engineering*, **19**(8), 667-691.

Simonsen BC, Friis-Hansen P, 2000. Theoretical and statistical analysis of ship grounding accidents. *Journal of Offshore Mechanics and Arctic Engineering, Transactions of the ASME*,**122**, 200-207.

Thomas PF, Wierzbicki T, 1992. Grounding damage to double hull tank vessels. *Proceedings of 2nd Int Offshore and Polar Engineering Conference (ISOPE)*, San Francisco, USA.

Vaughan H, 1980. The tearing strength of mild steel plate. *Ship Research*, **24**(2), 96-100.

Wang G, Arita K, Liu D, 2000. Behavior of a double hull in a variety of stranding or collision scenarios. *Marine Structures*, **13**, 147-187.

Wang G, Spencer J, Chen YJ, 2002. Review article: assessment of a ship's performance in accidents. *Marine Structures*, **15**, 313-333.

Yu Z, HuZ, WangG, LiuK, 2013a. An analysis of structural performances for bottom longitudinal girder and attached stiffeners during shoal grounding accident. *32nd International Conference on Ocean, Offshore and Arctic Engineering*,Nantes, France,OMAE2013-10167.

Yu Z, Hu Z, Wang G, 2013b. Plastic mechanism analysis of structural performances for stiffeners on bottom floor plating during shoal grounding accident. *Analysis and Design of Marine Structures. Proceedings of the 4th International Conference on Marine Structures*, Espoo, Finland.

Yu Z, HuZ, WangG, JiangZ, 2013c. Plastic mechanism analysis of structural performances for stiffeners on outer bottom plate during shoal grounding accident. *Collision and Grounding of Ships and Offshore Structures.Proceedings of the 6th International Conference on Collision and Grounding of Ships and Offshore Structures*, Trondheim, Norway, 17-19.

Zhang SM, 2002. Plate tearing and bottom damage in ship grounding. *Marine Structures*, **15**(2), 101-117.

Zeng J, Hu Z, Chen G, 2014. A steady-state plate tearing model for ship grounding over a cone-shaped rock. *Ships and Offshore Structures,(accepted)*.